Tackling Burst and Collapse for High-temperature Geothermal Well Casing Design

Gang Tao

C-FER Technologies (1999) Inc.

Keywords

Casing Design, Burst, Collapse, Elevated Temperature, Finite Element Analysis

ABSTRACT

Strain-based casing design approaches have been used for high-temperature thermal and geothermal well applications by accepting a limited amount of axial plastic strain while maintaining the casing integrity. However, there are still challenges in burst and collapse design for axially yielded casing strings since there are no analytical equations available in industry standards or recommended practices for calculating the post-yield casing burst and collapse strengths. There is a technical gap in the rationale for selecting the appropriate design methodologies and the associated design margins in post-yield casing burst and collapse design.

Finite Element Analysis (FEA) was conducted in this study to assist a technical investigation of the casing burst and collapse strengths in high-temperature geothermal wells. The FEA demonstrated the impact of key mechanical properties and the stress path on casing burst and collapse strengths at a few critical conditions through the thermal cycle. Based on the FEA results, extra design margins associated with the selected burst and collapse design equations were quantitatively evaluated. This study led to critical examinations of the applicability and limitations of the traditional burst and collapse design equations for high-temperature geothermal well applications. Physical testing is recommended for improving the confidence in casing burst and collapse design for high-temperature geothermal wells. The technical discussions presented in this paper are not only applicable for steel casings but also considered particularly valuable for corrosion resistant alloy (CRA) casings that have been used in geothermal wells, specifically due to the lack of test data and casing design methodologies for these casing candidates.

1. Introduction

In high-temperature thermal and geothermal wells, cemented casing strings may yield axially due to constrained thermal expansion and contraction during thermal cycles. Conventional stress-based design methodologies that limit the casing stress within the material's elastic range are no longer applicable in these scenarios. Alternatively, strain-based design approaches have been used by

accepting a limited amount of axial plastic strain while still maintaining the casing integrity. Since the first introduction of a post-yield thermal casing design methodology by Holliday (1969), additional research and design methodology improvements have been made in this area (Maruyama et al. 1990, Kaiser 2005, Nowinka et al. 2007, Suryanarayana and Krishnamurthy 2015). Due to the displacement-controlled nature of the thermal load in the axial direction, the casing string can still maintain structural integrity even as the load exceeds the yield limit as long as the amount of plastic deformation is tolerable by the casing connections. However, the pressure load (internal or external) is a load-controlled mechanism, and the strain-based design concept does not apply in the hoop direction of the casing. Therefore, burst and collapse design for axially yielded casing still needs to follow the traditional stress-based design approach to ensure that the casing pipe body has sufficient capacity to withstand the pressure load.

The most comprehensive downhole tubular design methodologies are documented in API TR 5C3 (API 2018). Design methods pertaining to internal pressure resistance include the historical Barlow equation, the triaxial yield equation and the ductile rupture model developed by Klever and Stewart (1998). Both the Barlow and triaxial yield equations predict the onset of yielding and are therefore theoretically invalid for casing strings where the stress exceeds the yield limit. The ductile rupture model incorporates large plastic deformation and predicts the actual rupture failure pressure of the pipe body subject to pure internal pressure. For collapse design, the API TR 5C3 includes both the historical API collapse equations and an advanced Klever-Tomano (KT) model (Klever and Tomano 2006). However, except for the elastic collapse equation, these equations are only applicable for ambient temperature conditions since the model parameters were calibrated based on ambient temperature test data. New Zealand's code of practice for deep geothermal wells (NZS 2403-2015) simply refers to API TR 5C3 for casing performance properties, including axial strength, internal pressure resistance and collapse resistance. The Alberta Industry Recommended Practice Volume 3 (IRP 3) (DACC 2012) developed by the Western Canadian oil and gas industry provides guidelines for thermal well casing design, most of which are also considered applicable for high-temperature geothermal well applications. The IRP 3 notes that there has been no conclusive evidence of casing burst failures in Western Canadian thermal operations and therefore does not provide clear guidance for burst design. On the other hand, the IRP 3 recognizes the limitations for thermal well casing collapse design and mentions that numerical modelling can be used to understand the response of casing strings in these scenarios.

A few published papers have discussed burst and collapse of casing in post-yield conditions that are relevant to thermal service tubulars. Derived from the fundamental physics, Huang and Pattillo (1982) developed a collapse model incorporating the post-yield material stress-strain response and axial stress in the cross-sectional bending stiffness. This approach differs from the method in API TR 5C3 that accounts for the axial stress effect in the collapse strength using the von Mises equivalent stress formula, and therefore offers the opportunity to treat scenarios where the casing stress exceeds the yield limit. As part of an experimental study on thermal service casing performance by Maruyama et al. (1990), collapse tests conducted in this program included as-rolled K55 casing samples under constant axial tensile loads exceeding the yield limit. These casing samples showed an appreciable amount of collapse resistance and provided some confidence for such challenging applications. Dall'Acqua et al. (2013) investigated this topic using FEA and concluded that the ductile rupture strength of a cemented casing string is independent of the initial stress or strain. While for collapse, the authors acknowledged the more complex nature

of the pipe response and the impact of path dependency on collapse strength and therefore did not provide a recommendation for a collapse design method.

Although temperature derating of some material properties may be considered appropriate in traditional burst and collapse design equations, this approach can violate the technical basis of these equations and lead to unknown risks in the casing design. Moreover, previous studies have shown pronounced strain rate dependency of casing materials at elevated temperatures which can significantly affect the casing strength (Tao et al. 2021). Traditional material testing and casing design approaches do not capture the strain rate effect, which further complicates the casing design.

The objective of this paper is to improve the understanding of casing response under pressure loads and the corresponding burst and collapse strengths in high-temperature wells. Using FEA on a 13-3/8", 68 ppf, L80 casing example, this study led to critical examinations of the applicability and limitations of the traditional burst and collapse design equations for high-temperature geothermal well applications. Physical testing is recommended for improving the confidence in casing burst and collapse design for high-temperature geothermal wells. The technical discussions presented in this paper are not only applicable for steel casing but also considered particularly valuable for corrosion resistant alloys (CRA) casing that have been used in geothermal wells, specifically due to the lack of test data and casing design methodologies for these casing candidates.

2. Elevated Temperature Effects on Burst and Collapse Strengths

Elevated temperatures such as those in high-temperature geothermal wells are known to significantly reduce the strength of Oil Country Tubular Goods (OCTG). Tao et al. (2021) conducted a comprehensive study on the effects of elevated temperature on OCTG materials and the resulting impact on tubular strength. In general, elevated temperatures cause a reduction of several key mechanical parameters that can significantly affect the burst and collapse strength, including the Young's modulus, yield strength (YS) and ultimate tensile strength (UTS). Temperature derating factors of these key parameters such as those provided in the New Zealand's code of practice for deep geothermal wells (NZS 2403-2015) are commonly used in elevated temperature casing design. In addition, Tao et al. (2021) demonstrated a pronounced strain rate effect at elevated temperature which significantly affects the tubular performance.

When the casing material has sufficient toughness (i.e. when toughness reduction due to various corrosion mechanisms is not a significant concern), the casing burst is ductile and the burst strength primarily depends on the stress-strain relationship within the high plasticity region (i.e., UTS and strain hardening property). Temperature derating on the UTS directly affects the ultimate rupture strength of the casing, while the temperature effect on strain hardening response only has a secondary effect on the ductile rupture strength. Collapse is an instability failure mode which depends on the cross-sectional stiffness of the casing. Collapse models derived from fundamental physics such as the KT model in API TR 5C3 and the model by Huang and Pattillo (1982) indicate that the key parameters affecting the cross-sectional stiffness include the Young's modulus, Poisson's ratio, the post-yield stress-strain response within the small plasticity region (i.e., YS and strain hardening property), as well as the axial stress. Therefore, elevated temperature effects on the Young's modulus and the post-yield stress-strain response within the small plasticity region dominates the reduction of the casing collapse strength. Poisson's ratio has a negligible effect on casing collapse strength at elevated temperature, due to the small temperature dependency of Poisson's ratio and the secondary effect Poisson's ratio has on collapse strength. The thermally-

induced axial stress also affects the casing cross-sectional stiffness as explicitly shown in the collapse model by Huang and Pattillo (1982), which significantly complicates the elevated temperature effects on collapse strength.

3. Stress and Strain in Cemented Casing Strings

Since the casing string is cemented in place, temperature variations in a geothermal well will introduce a significant axial load in the casing string as it's prevented from axial expansion and contraction. In addition, the internal or external pressure change will also cause axial stress change in an axially constrained casing string due to Poisson's effect. The stress and strain in an axially constrained casing string have a significant impact on the burst and collapse strengths. Therefore, it is important to review the fundamental stress and strain conditions in constrained casing for this investigation. Note that the beneficial effects of the radial support from the cement sheath are not considered in this study, as a common practice in general casing design.

Since it's more convenient to describe the elastic-plastic stress and strain responses of the pipe in the incremental form, stress and strain rates are used in the description below. As the most important strain component in a geothermal well casing string, the total axial strain rate includes three components (elastic, plastic and thermal) as:

$$\dot{\epsilon_a} = \dot{\epsilon}_a^e + \dot{\epsilon}_a^p + \alpha\dot{T} \tag{1}$$

where $\dot{\epsilon}_a^e$ and $\dot{\epsilon}_a^p$ are elastic and plastic axial strain rates, respectively, α is the coefficient of thermal expansion and $\dot{T}$ is the rate of temperature change. For a cemented casing string, the total axial strain rate is zero:

$$\dot{\epsilon}_a^e + \dot{\epsilon}_a^p + \alpha\dot{T} = 0 \tag{2}$$

The elastic axial strain rate is a function of the rates of the three normal stresses in the pipe body according to the generalized Hooke's law:

$$\dot{\epsilon}_a^e = \frac{1}{E}[\dot{\sigma_a} - v(\dot{\sigma_h} + \dot{\sigma_r})] \tag{3}$$

where $\dot{\sigma_a}$, $\dot{\sigma_h}$ and $\dot{\sigma_r}$ are the rates of the stresses in the axial, hoop and radial directions, respectively, E is Young's modulus and v is Poisson's ratio.

As per the classical metal plasticity theory (Chakrabarty 2006), the plastic strain rate is proportional to the corresponding deviatoric stress following the associated flow rule, and the axial plastic strain rate is expressed as:

$$\dot{\epsilon}_a^p = \frac{\dot{\epsilon}}{\sigma}\left[\sigma_a - \frac{1}{2}(\sigma_h + \sigma_r)\right] \tag{4}$$

where σ_a, σ_h and σ_r are the stresses in the axial, hoop and radial directions, respectively, σ is the von Mises equivalent stress and $\dot{\epsilon}$ is the equivalent plastic strain rate. The relationship between σ and ϵ follows the true stress vs. plastic strain relationship from uniaxial tensile coupon test data.

Substituting Eqs. (3) and (4) into Eq. (2), the axial stress rate can be expressed as:

$$\dot{\sigma_a} = -E\alpha\dot{T} + v(\dot{\sigma_h} + \dot{\sigma_r}) - E\frac{\dot{\epsilon}}{\sigma}\left[\sigma_a - \frac{1}{2}(\sigma_h + \sigma_r)\right] \tag{5}$$

Eq. (5) establishes the general form of the axial stress response of a cemented casing string in a geothermal well.

At a constant temperature ($\dot{T} = 0$) and when the pipe body stress is within the elastic limit ($\dot{\epsilon} = 0$), Eq. (5) only has the elastic component as:

$$\dot{\sigma_a} = v(\dot{\sigma_h} + \dot{\sigma_r}) \tag{6}$$

When the equivalent stress exceeds the yield limit, the axial stress rate is not only a function of the hoop and radial stress rates but also the current stress condition in the pipe:

$$\dot{\sigma_a} = v(\dot{\sigma_h} + \dot{\sigma_r}) - E\frac{\dot{\epsilon}}{\sigma}\left[\sigma_a - \frac{1}{2}(\sigma_h + \sigma_r)\right] \tag{7}$$

The hoop and radial stresses are functions of the internal and external pressures under equilibrium conditions. According to Stewart et al. (1994), the average hoop and radial stresses over the pipe wall thickness are:

$$\sigma_h = \frac{R'}{t'}(p_i - p_e) - \frac{1}{2}(p_i + p_e) \tag{8}$$

$$\sigma_r = -\frac{1}{2}(p_i + p_e) \tag{9}$$

where, p_i and p_e are the internal and external pressures, respectively. R' and t' are the deformed mean radius (average of the outer radius and the inner radius) and deformed wall thickness of the pipe, respectively. For elastic deformation of steel pipes, undeformed pipe dimensions may be used.

4. Analysis and Results

FEA was performed on a 13-3/8", 68 ppf, L80 casing pipe body at selected critical conditions during a thermal cycle (25°C~325°C). The commercial FEA program Abaqus 2023 (Dassault Systèmes 2023) was used. The pipe body was modeled with generalized 2D plane strain elements. Various assumptions and modeling approaches were used in the burst and collapse analyses, as described below.

The L80 casing material constitutive model was developed based on coupon tensile tests conducted at different temperatures across the thermal cycle temperature range. The material model has a temperature dependent elastic-plastic relationship with an assumed isotropic hardening rule. The static stress-strain curves that reflect the long-term response of the casing material under infinitely slow strain rate were used to define the post-yield stress-strain relationship, so the analysis provided a conservative estimation of the casing strength. The method to calibrate the static stress-strain curve using tensile coupon test results with stress relaxation periods is described by Tao et al. (2021). Figure 1 shows the static stress-strain curves of the L80 material at ambient and peak temperatures. Note that the temperature derating of YS and UTS from static stress-strain curves is greater than that in the NZS 2403-2015 due to the stress relaxation behavior (i.e., strain rate effect). A constant coefficient of thermal expansion of 14 με/°C as suggested in ISO/PAS 12835 (2013) was used.

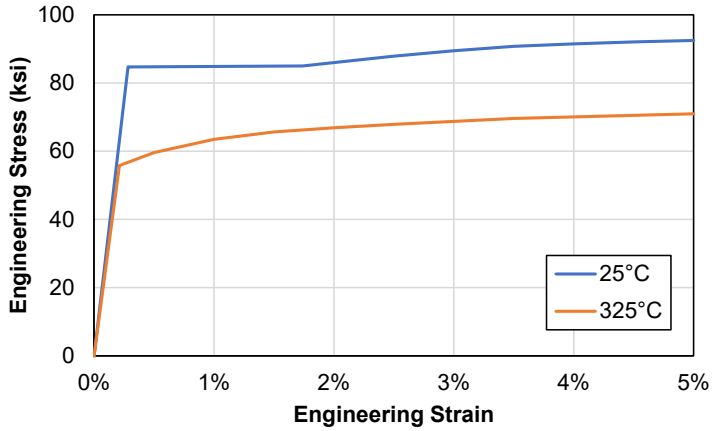

Figure 1: Static Engineering Stress-strain Curves of the L80 Material

4.1 Thermal Cycle Analysis

Figure 2 shows the response of the axial stress in the axially constrained casing (i.e., cemented casing) FEA model to temperature over the first thermal cycle. Since the casing material model was based on static stress-strain curves, the axial stress response followed the orange curve in the chart after the initial yielding at around 200°C. For comparison, a conceptual dashed blue curve representing the axial stress response of a rapidly heated casing string was also plotted. Due to the strain rate dependency of the casing material, the fast heating of the casing string resulted in stress relaxation over time at the peak temperature, as observed in lab tests (Droessler et al. 2021). When the well is quenched, such as during water injection or a workover, the temperature drop would lead to an elastic unloading of the casing string. Further temperature reduction causes axial tension along the casing string. In subsequent thermal cycles, the axial stress response closely follows that of the cooling curve if there is no plastic deformation in the casing string during cooling (Droessler et al. 2021). At the end of the cooling phase, the FEA model shows that the casing string remains within its elastic limit.

Casing burst and collapse analyses were conducted at three critical conditions:

- At ambient temperature before heating - casing is in the elastic region with zero axial stress;
- At peak temperature during well production - casing is under compression beyond the yield limit; and
- At ambient temperature during well shut-in - casing returns to the elastic region and is under tension.

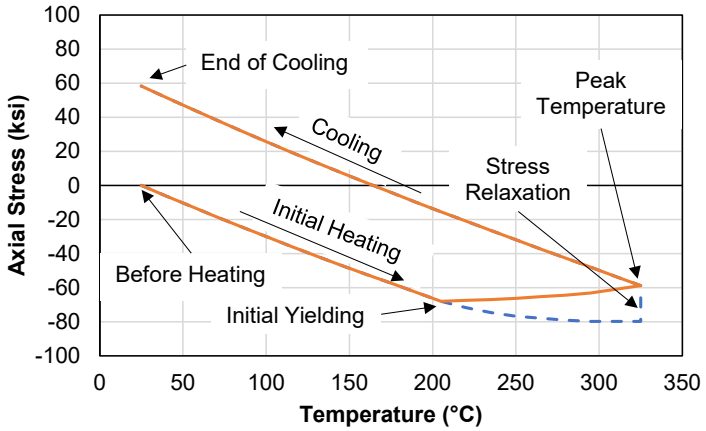

Figure 2: Casing Axial Stress During the First Thermal Cycle

4.2 Burst Analysis

The objective of the burst analysis was to estimate the ductile rupture strength of the casing, which is in contrast to the pressure capacity at the onset of yielding. The burst analysis model assumed nominal casing dimensions and predicted the ductile rupture strength associated with the global plastic instability failure of pipes as in the analytical burst models (Klever and Stewart 1998, Zhu and Leis 2006). Three cases were analyzed representing the cemented casing string before heating, at the peak temperature, and after cooling. Each case included one or multiple load steps, including an initial thermal load step when applicable (i.e., either heating to peak temperature or cooling to ambient) followed by the final burst analysis step. Two additional reference cases were analyzed considering an axisymmetric model with welded end caps (i.e., capped-end condition) at both ambient and peak temperatures. In the burst analysis step, an internal pressure was applied on the inner surface of the pipe while the external pressure was kept at zero. The analysis was performed using the modified Riks method, a special numerical technique to solve instability problems.

4.2.1 FEA Results

Figure 3 presents the analysis results showing the internal pressure response as a function of equivalent plastic strain for all five cases. The peak values in the curves are the plastic instability points representing the maximum internal pressure capacity that the casing can sustain. The results show that the ultimate burst strength is almost identical for the load cases at the same temperature. The different load history and/or boundary condition showed an impact on the pipe response at low plastic strain levels (<1%) beyond which the response converged among the analysis cases.

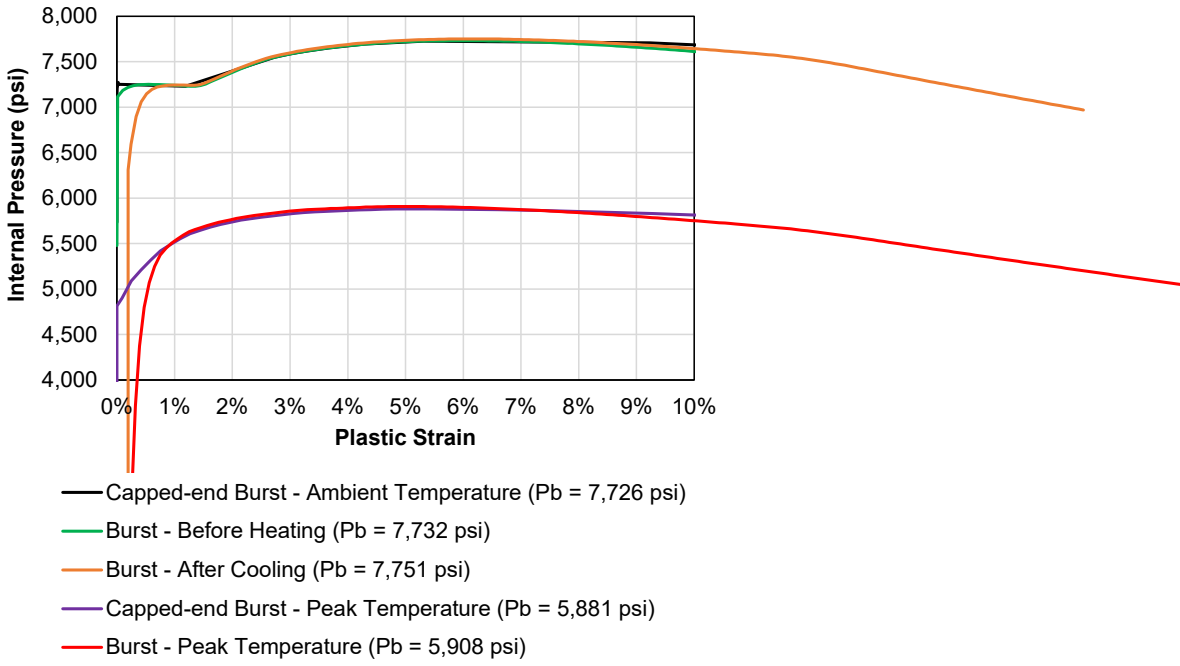

Figure 3: Internal Pressure vs. Plastic Strain

The convergence of the pressure vs. plastic strain response at large plastic strain levels can be explained by the pipe stress and deformation response. When the pipe stress is within the elastic limit, the change of axial stress follows Eq. (6). Substituting Eqs. (8) and (9) into Eq. (6) and setting $p_e = 0$, the axial stress rate can be expressed as a function of the internal pressure rate as:

$$\dot{\sigma_a} = v\left(\frac{R'}{t'} - 1\right)\dot{p_i} \tag{10}$$

From Eq. (8), the hoop stress rate as a function of internal pressure rate is:

$$\dot{\sigma_h} = \left(\frac{R'}{t'} - \frac{1}{2}\right)\dot{p_i} \tag{11}$$

From Eqs. (10) and (11), it's shown that the rate of stress change between the axial and hoop components is approximately equal to the Poisson's ratio (0.3) for typical OCTG pipes. This relationship may also be obtained from Eq. (6) considering that the radial stress component is much less than the axial and hoop stress components.

When the stresses reach the yield surface, further changes in the axial and hoop stresses no longer follow the proportional relationship since the axial stress rate now follows Eq. (7) instead, while the hoop stress is still determined by the equilibrium condition in Eq. (11). Substituting Eqs. (8) and (9) into Eq. (7) and setting $p_e = 0$, the axial stress rate is:

$$\dot{\sigma_a} = v\left(\frac{R'}{t'} - 1\right)\dot{p_i} - E\frac{\dot{\varepsilon}}{\sigma}\left[\sigma_a - \frac{1}{2}\left(\frac{R'}{t'} - 1\right)p_i\right] \tag{12}$$

Eq. (12) shows that the axial stress rate is not only dependent on the rate of internal pressure change but also the current stress condition in the pipe and the post-yield stress-strain response. The axial stress in Eq. (12) may be solved incrementally in a spreadsheet or by FEA.

Figure 4 shows the pipe body stress path in the axial vs. hoop stress space in the burst analysis step for the three cemented casing string cases. For the two cases where the pipe stress started within the elastic range, upon internal pressure loading the axial stress vs. hoop stress relationship follows an almost straight line as discussed above. Upon yielding, the stress path for all three cases converged along the corresponding initial yield surfaces to the stress path of the capped-end condition (axial stress vs. hoop stress ≈ 0.5). This behavior was also discussed by Stewart et al. (1994) and Dall'Acqua et al. (2013). The pipe ductile rupture strength is driven by the non-linear response of both pipe wall thinning and the material strain hardening. Both of these effects were relatively small before the pipe stress converged to the stress path of the capped-end condition (at 1%~2% plastic strain). After the pipe stresses converged, the incremental pipe deformation is mostly plastic and is almost identical among these cases (i.e, the incremental plastic strain follows the associated flow rule and the deviatoric stresses are the same). As such, the pipe ductile rupture strength of the different cases is very close to that of the capped-end condition.

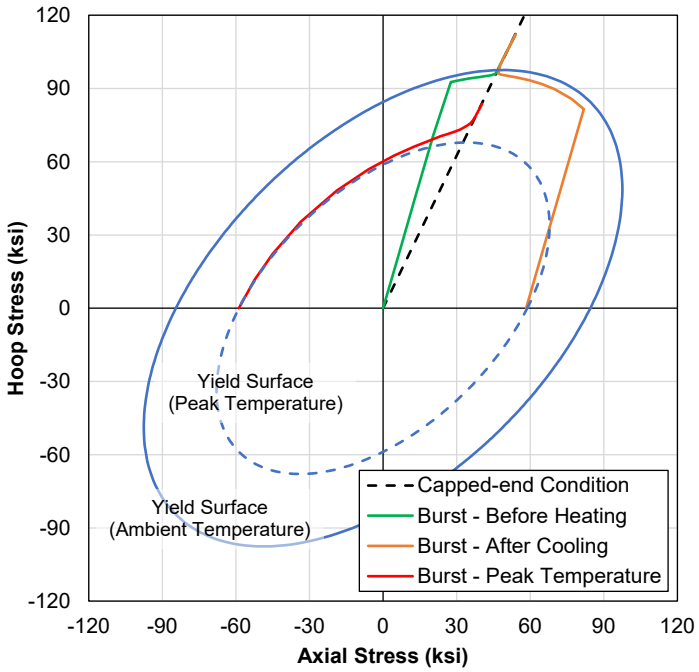

Figure 4: Casing Stresses Under Internal Pressure

At high hoop stresses, the post-yield stress points in Figure 4 were slightly below the initial yield surface for the two ambient temperature cases. This was due to the influence of the small radial stress component on triaxial yielding that's not shown in this plot. Also note that the yield surface at the peak temperature is slightly larger than the virgin yield surface of the casing material at that temperature, and it represents the current yield surface after a small amount of strain hardening associated with the plastic deformation during the heating process, assuming an isotropic hardening rule.

4.2.2 Burst Design Approach Evaluation

It is important to note that the shape of the yield surface has a great impact on the ductile rupture strength of the pipe. The KS ductile rupture model uses the average of the solutions from the von Mises and Tresca yield theories based on experimental evidence (Klever and Stewart 1998).

Motivated by this finding, Zhu and Leis (2006) further developed a new average shear stress yield (ASSY) criterion with a yield locus between the von Mises and Tresca yield loci, as shown in Figure 5.

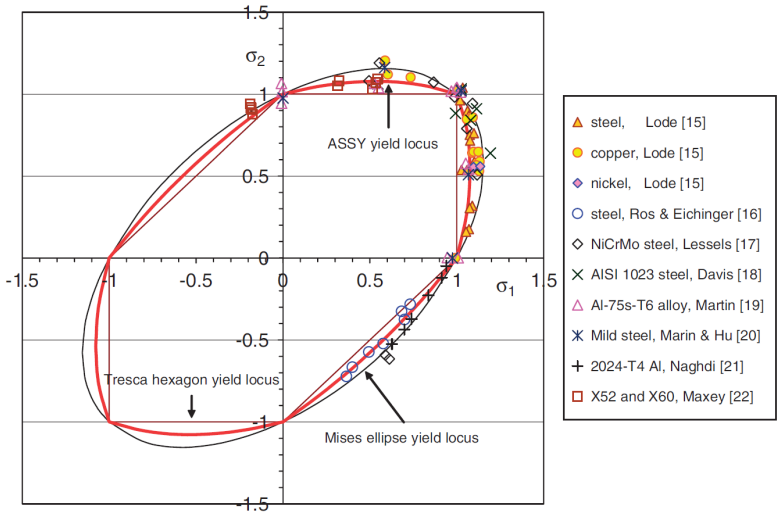

Figure 5: Comparison of Three Yield Criteria and Experimental Data (Zhu and Leis 2006)

The ASSY yield theory led to a similar ductile rupture strength solution for a capped-end pipe as the KS equation. Since the FEA-predicted ultimate burst strength is based on the von Mises yield criterion, a scale factor was proposed by Tao (2023) to improve the FEA prediction accuracy. The scale factor is the ratio of the burst pressure solutions between the ASSY yield theory and the von Mises yield theory for the capped-end pipe:

$$f(n) = \left(\frac{2+\sqrt{3}}{4}\right)^{n+1} \tag{13}$$

where n is the Ludwik strain hardening exponent (1909).

For the L80 casing material considered in this study, the calibrated n is 0.11 at ambient temperature and 0.09 at the peak temperature of 325°C. Multiplying the FEA-predicted burst pressure by the scale factor, the corrected burst pressure values are presented in Figure 6. The corrected values are considered to be a reasonable prediction of the actual burst capacity of the casing and are used to assess the extra design margin. Using the historical Barlow equation in API TR 5C3, the internal pressure rating for both ambient and peak temperatures are obtained as shown in Figure 6. Note that the nominal YS and a 12.5% wall thickness tolerance specified in API Specification 5CT (2018) were used in the calculation. A YS derating factor of 0.83 for L80 at 325°C (as per NZS 2403:2015) were considered for the case at the peak temperature. The extra burst design margin (i.e., the difference between the ductile rupture strength and the internal yield pressure rating) is 42% for all load cases at ambient temperature and 31% for all load cases at the peak temperature. Note that the reduced design margin at the peak temperature is due to the reason that the YS derating factor used in the calculation might not have considered the effects of stress relaxation.

In general, burst design using the Barlow equation seems to be acceptable for cemented casing strings in post-yield conditions. It is important to use YS derating factors that consider the stress relaxation effect to ensure a sufficient design margin is maintained at elevated temperatures. In

addition, it is recommended that coupon tensile tests with stress relaxation periods be conducted at elevated temperatures to measure the static UTS and strain hardening properties that are required for estimating the ductile rupture strength and to better quantify the design margin.

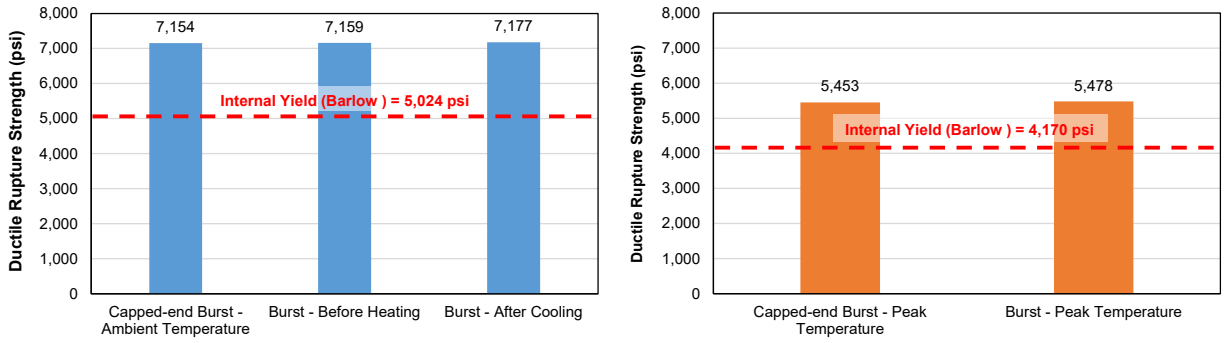

Figure 6: Predicted Ductile Rupture Strength

It is important to note that test results have shown a significant change of the steel material response after being plastically cycled (Kaiser et al. 2008). The yield surface after cooling of the first thermal cycle can be significantly different from that before heating, even at the same temperature. Although the casing material model in the FEA has a temperature dependency, it does not capture the material property change after thermal cycle loading. In particular, the yield plateau as shown in Figure 1 that is often observed in quenched and tempered pipe would disappear and the elastic-plastic transition becomes round-kneed. The material YS also reduces in tension after plastic deformation in compression due to the Bauschinger effect. In general, the plastic deformation during a thermal cycle can significantly change the yield surface, including expansion and contraction, translation and distortion (Khan and Huang 1995). The effect of yield surface change on the ductile rupture strength should be further investigated.

4.3 Collapse Analysis

The collapse FEA model considered an initial casing ovality of 0.217% based on the statistical mean value of the OCTG production quality data in API TR 5C3, while other manufacturing imperfections were ignored. The analysis matrix included seven cases:

- Collapse – Before Heating - cemented casing at ambient temperature before heating.
- Collapse – After Cooling - cemented casing at ambient temperature after cooling.
- Collapse – LT (Reference Case) - unconstrained casing (zero axial stress) at ambient temperature representing the collapse test condition specified in API TR 5C3 Annex I.
- Collapse – LT with Tension - casing collapse under a constant tensile stress equal to that in the cemented casing after cooling.
- Collapse – Peak Temperature - cemented casing at peak temperature.
- Collapse – HT (Reference Case) - unconstrained casing (zero axial stress) at peak temperature representing the collapse test condition specified in API TR 5C3 Annex I.
- Collapse – HT with Compression - casing collapse under a constant compressive stress equal to that in the cemented casing at the peak temperature.

Each analysis case included one or multiple load steps, including an initial thermal or mechanical load step followed by the final collapse analysis step. In the collapse analysis step, an external pressure was applied on the outer surface of the pipe while the internal pressure was kept at zero. The FEA collapse analysis was also performed using the modified Riks method.

4.3.1 FEA Results

Figure 7 shows the results of the external pressure vs. ovality response for the four cases at ambient temperature, where the collapse point is represented by the peak value in the curve. The collapse strength of the axially constrained case before heating (Collapse – Before Heating) is marginally higher than that of the axially unconstrained case (Collapse – LT). While both cases under tension showed expected collapse strength reductions.

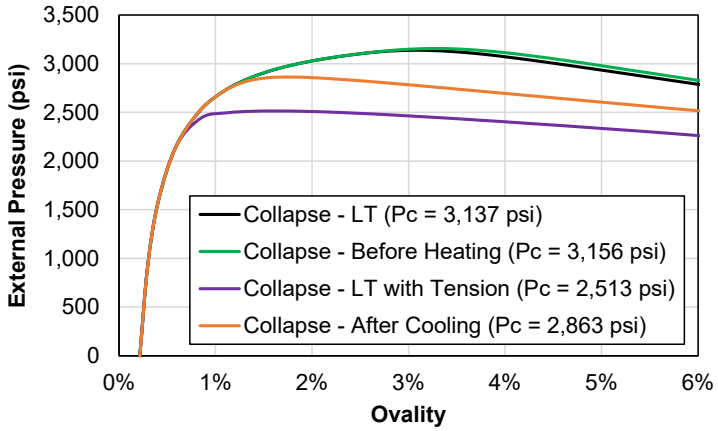

Figure 7: External Pressure vs. Pipe Ovality (Ambient Temperature before Heating)

A close review of the global pipe body stresses can explain the variation of collapse strength among these cases. The global pipe body stresses are determined following the governing equations described in Section 3 of this paper by assuming a pure external pressure applied on the outer surface of a perfectly round pipe. The global pipe body stresses do not reflect the actual stress condition of a real casing where, due to imperfections, pipe ovalization would always occur under external pressure which introduces additional cross-sectional bending stresses. However, the global pipe body stress state provides insight into the overall stress condition in the casing for the purpose of investigating impacts on the casing collapse strength.

Within the elastic limit, the change of axial stress follows Eq. (6). Substituting Eqs. (8) and (9) into Eq. (6) and setting $p_i = 0$, the axial stress rate can be expressed as a function of the external pressure rate as:

$$\dot{\sigma_a} = -v\left(\frac{R'}{t'} + 1\right)\dot{p}_e \tag{14}$$

From Eq. (8), the hoop stress rate as a function of internal pressure rate is:

$$\dot{\sigma_h} = -\left(\frac{R'}{t'} + \frac{1}{2}\right)\dot{p}_e \tag{15}$$

Similar to the cases under pure internal pressure loading, the rate of stress change between the axial and hoop components is approximately equal to the Poisson's ratio (0.3).

Using Eqs. (14) and (15) and considering the initial axial stress state, the global pipe body stress paths in the collapse analysis step for the two axially constrained cases (i.e., Collapse – Before Heating and Collapse – After Cooling) are plotted in Figure 8. The stress paths for the two cases under constant axial stress (i.e., Collapse – LT and Collapse – LT with Tension) are also plotted for comparison. The results clearly demonstrate the detrimental effect of tensile stress on collapse strength as accounted for by analytical collapse strength prediction models. The axial constraint from the cement leads to a beneficial effect for the cemented casing with reduced axial tensile stress or increased axial compressive stress (Poisson's effect), which results in an increased collapse strength compared to the cases under constant axial stress.

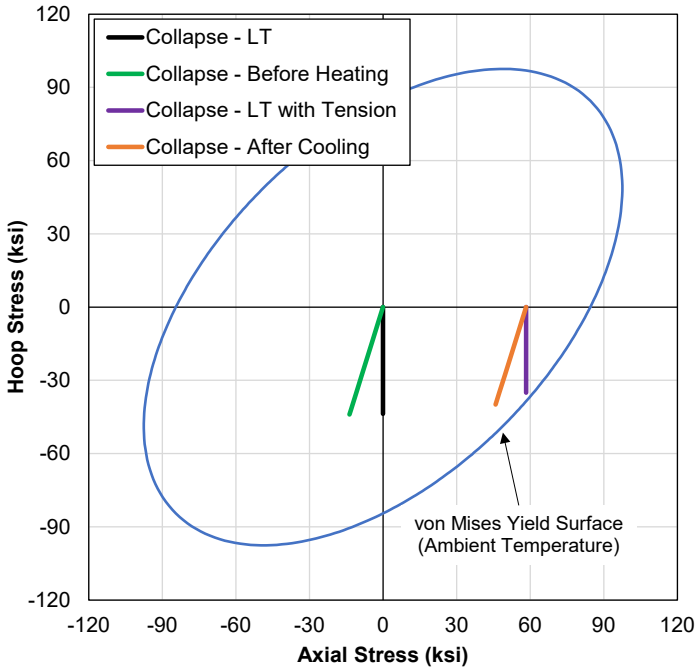

Figure 8: Casing Stresses Under External Pressure (Ambient Temperature)

At high tensile stresses, the casing reaches its collapse limit due to local yielding when the global stress state approaches the yield surface. As previously discussed in the burst analysis, the yield surface after cooling can be significantly different than before heating, which can significantly affect the collapse strength of the casing. Therefore, attention should be paid to ensure that an extra safety margin is applied to account for the uncertainties due to modeling assumptions and limitations. Ultimately, full-scale collapse tests of casing samples that have been subjected to representative constrained thermal cycle loading would provide confidence to validate the model predictions.

Figure 9 shows the analysis results with external pressure vs. ovality response for the three cases at the peak temperature. Compared to the axially unconstrained case (Collapse – HT), the high compressive stress leads to reduced collapse strength. In addition, between the two cases under high compression, the cement confinement showed a detrimental effect on the collapse strength, which is in contrast to the cases at ambient temperature. Most importantly, the scenario where the casing has already yielded still shows a significant amount of collapse strength. The results are truly unintuitive.

Again, a careful review of the global pipe stresses can facilitate the interpretation of the predicted collapse strength results. Figure 10 shows the stress path for the three analysis cases. The von Mises yield surface at the peak temperature after a small amount of strain hardening was plotted as a reference. At the beginning of the collapse analysis step, the stress state is located on the yield surface. For the two cases under initial axial compressive stress, the external pressure results in an elastic unloading whereas the stress state moved towards the inside of the yield surface. The elastic unloading leads to a recovery of the material elastic stiffness, which is the main contributor to the collapse strength. This behavior is reflected in Figure 9 where the initial cross-sectional stiffness reflected by the slope of the external pressure vs. ovality curve is almost identical among the three cases up to a pressure of ~1700 psi. Beyond this point, local yielding in the axially constrained case (Collapse – Peak Temperature) started to quickly reduce the cross-sectional stiffness of the pipe model.

As shown in Figure 10, further increases in the external pressure in the axially constrained case causes the global stress state to reach the yield surface again leading to final collapse. While for the other two cases, the global pipe stress state at the moment of collapse is still some distance from the yield surface. In general, a key learning from this investigation is that the global pipe body stress state at the peak temperature is on or close to the yield surface, which results in a great uncertainty of the pipe cross-sectional stiffness and collapse strength. As discussed previously, thermal cycles can significantly change the yield surface, which would in turn affect the collapse strength. Therefore, FEA-predicted collapse strength in this scenario needs to be carefully reviewed and an extra safety margin should be applied to account for prediction uncertainties due to modeling assumptions and limitations. Further research consisting of a carefully designed test program including characterization of the material behavior and full-scale collapse test of casing samples under representative thermal cycle load conditions is warranted to improve the confidence in casing collapse design for such challenging conditions. This is even more critical for CRA casings that have been used in geothermal wells, mainly due to the lack of test data and the more complex pipe structural response resulting from the anisotropic material property.

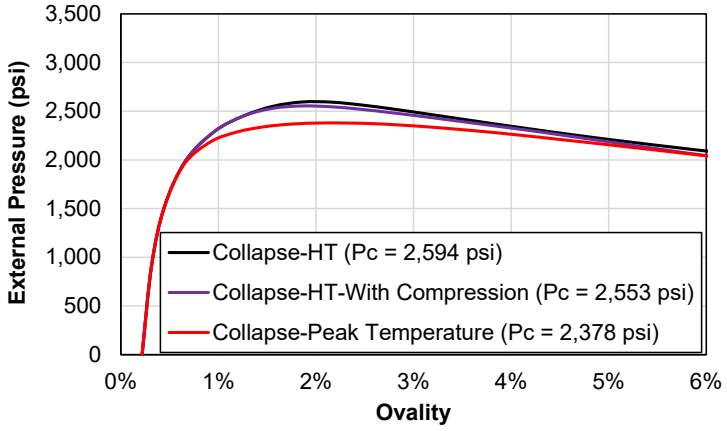

Figure 9: External Pressure vs. Pipe Ovality (Peak Temperature)

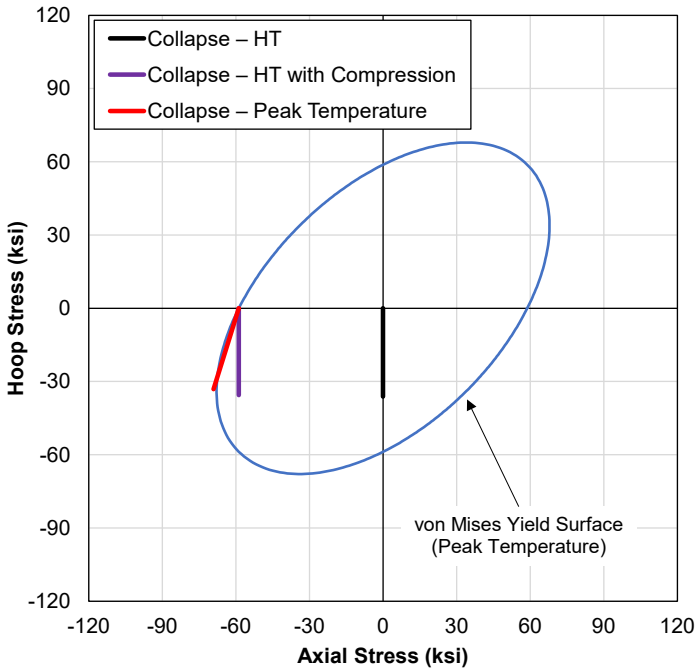

Figure 10: Casing Stresses Under External Pressure (Peak Temperature)

4.3.2 Collapse Design Approach Evaluation

Figure 11 presents the FEA-predicted collapse strength for all cases. For comparison, either the historical API design equations or the KT equation can be used to calculate the design collapse strength at ambient temperature. As an example, the API collapse rating (calculated by the historical API collapse equations) and the collapse strength adjusted for the effects of the axial tensile stress are shown in Figure 11. The extra design margin (the difference between the FEA-predicted collapse strength and the API rating) is 40% for the case at ambient temperature before heating, and 89% for the case after cooling. It appears that the API rating adjusted for the axial stress gives an extra design margin for the case after cooling. However, it must be recognized that the design margin has a high uncertainty due to the sensitivity of the yield surface shape and the relative position of the pipe body stress on collapse strength as discussed above. No attempt was made to use the API equations to predict the collapse rating at the peak temperature, since this approach is invalid due to the elevated temperature and post-yield stress state.

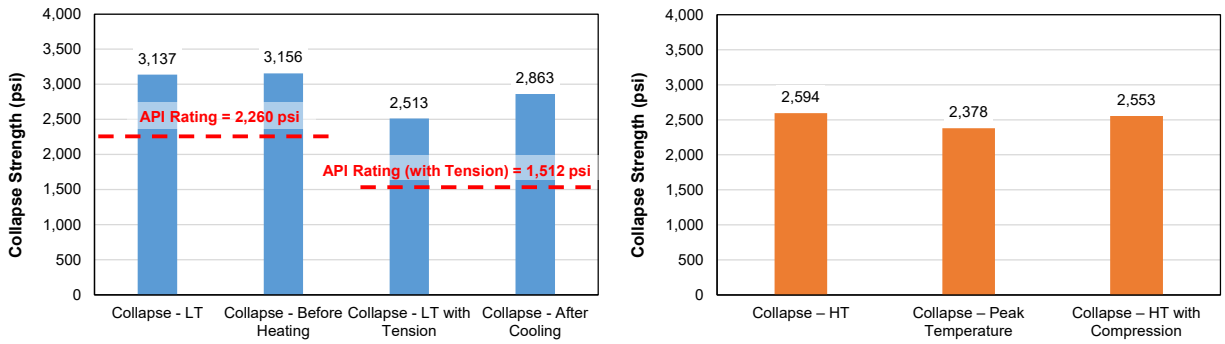

Figure 11: Predicted Collapse Strength

It should be noted that this study did not consider the impact of other imperfections on collapse strength of thermal well casing. The study by Dall'Acqua et al. (2013) showed that even low net external pressure can lead to casing ovalization and loss of wellbore access when combined with thermally induced axial strain and where there is insufficient cement radial support. These are additional factors that should be considered for casing collapse design for high-temperature geothermal wells.

5. Conclusions and Recommendations

An in-depth investigation was conducted to understand the casing stress and strain response under pressure loads and the corresponding burst and collapse strengths at load conditions representative of high-temperature thermal or geothermal wells. The key findings and conclusions are summarized below:

- The ductile rupture strength of a cemented casing string is nearly independent of its load history and can be closely predicted by analytical equations for the capped-end condition.
- Traditional burst design equations that predict the onset of yielding (e.g. Barlow equation) can still be used for burst design of cemented casing strings in post-yield conditions.
- Calculating internal pressure rating at elevated temperatures should consider the stress relaxation effect to ensure a sufficient burst design margin is maintained. Tensile coupon tests with stress relaxation periods at elevated temperatures are recommended to measure the static UTS and strain hardening properties to better quantify the burst design margin.
- Historical API equations or the KT equation may be used to estimate the casing design collapse strength at ambient temperature during a thermal cycle. However, the design margin for cases after thermal cycles can be highly uncertain, since the yield surface changes after the thermal cycle and the pipe body stress state relative to the yield surface can significantly affect the collapse strength.
- Neither historical API equations or the KT equation should be used for elevated temperature collapse design. Numerical modeling such as FEA can properly capture the temperature-dependent material properties and load path for these cases. One exception would be the case that the pipe body stays within the elastic range and the collapse mode is primarily elastic collapse as has been reported for titanium casing (MacDonald and Gram 2021, Tao et al. 2022).
- The casing collapse strength showed a strong dependence on the pipe body stress path relative to the yield surface. Therefore, FEA-predicted collapse strength at critical conditions during the thermal cycle needs to be carefully reviewed and an extra safety margin should be applied to account for prediction uncertainties due to modeling assumptions and limitations.

This study led to the following recommendations for improving casing burst and collapse design methodologies for high-temperature thermal or geothermal wells:

- Further research with a carefully designed test program is warranted to improve the confidence in casing design for challenging high-temperature applications.
    - Coupon tests of casing samples that have been thermally cycled with axial constraint should be conducted to characterize the material properties at critical

conditions during the thermal cycle, such as at the peak temperature and the end of cooling.
    - Full-scale collapse tests of casing samples at critical conditions during the thermal cycle, such as those examined in this study, should be performed.
    - Using the test results, collapse strength prediction models should be improved to address the critical scenarios in thermal and high-temperature geothermal wells.
- Fundamental study of the structural behavior of CRA casings that have been used in geothermal wells should be conducted.
    - Material coupon tests and full-scale collapse tests similar to those conducted for OCTG products should be performed to examine the applicability of the commonly used casing design equations for CRA products.
    - The outcome of the study would facilitate necessary adjustment of these design equations for CRA casings when applicable.
    - The technical discussions presented in this paper should also be considered in future research to improve the CRA casing designs for high-temperature geothermal well applications.

Acknowledgement

The authors sincerely appreciate the support received from C-FER Technologies (1999) Inc. for the preparation of this paper and in authorizing its publication.

REFERENCES

API Specification 5CT, Casing and Tubing, tenth edition. 2018. Washington, DC: API.

API Technical Report 5C3, Calculating Performance Properties of Pipe Used as Casing or Tubing, seventh edition. 2018. Washington, DC: API.

Chakrabarty, J. 2006. *Theory of Plasticity*, third edition. Oxford, United Kingdom: Butterworth-Heinemann.

Dall'Acqua, D., Hodder, M., and Kaiser, T.M.V. 2013. Burst and Collapse Responses of Production Casing in Thermal Applications. *SPE Drilling and Completions.* 28: 93–104. doi: https://doi.org/10.2118/151810-PA.

Dassault Systèmes. Simulia User Assistance 2023.

Drilling and Completion Committee (DACC) IRP Volume #3. In Situ Heavy Oil Operations: An Industry Recommended Practice (IRP) for the Canadian Oil and Gas Industry, #3.2 edition. 2012. Calgary, Alberta, Canada: Enform Canada.

Droessler, M., Tao, G., Hamilton, K., Skelton, B. and Yoshikawa, M. 2021. Casing Connection Evaluation for High-temperature Geothermal Applications – A Case Study. Presented at the World Geothermal Congress 2020+1, Reykjavik, Iceland, April – October.

Holliday, GH. 1969. Calculation of allowable maximum casing temperature to prevent tension failures in thermal wells. Proceedings of the ASME Petroleum Mechanical Engineering Conference; 1969 Sep 21; Tulsa, OK. CONF 690962.

Huang, N.C. and Pattillo, P.D. 1982. Collapse of Oil Well Casing. ASME. *J. Pressure Vessel Technol*. February; 104(1): 36–41. https://doi.org/10.1115/1.3264183.

ISO: Qualification of Casing Connections for Thermal Wells, ISO/PAS 12835:2013(E), ISO, Geneva, Switzerland (2013).

Kaiser, T.M.V. 2005. Post-Yield Material Characterization for Strain-Based Design. SPE J. 14 (1): 128-134. SPE-97730-PA. https://doi.org/10.2118/97730-PA.

Kaiser, T.M.V., Yung, V.Y.B., and Bacon, R.M. 2008. Cyclic Mechanical and Fatigue Properties for Oil-Country-Tubular-Goods Materials. *SPE Journal*. 13: 480–486. doi: https://doi.org/10.2118/97775-PA.

Khan, A.S. and Huang, S. 1995. *Continuum Theory of Plasticity*. New York, USA: John Wiley & Sons, Inc.

Klever, F.J. and Tamano, T. 2006. A New OCTG Strength Equation for Collapse Under Combined Loads. *SPE Drilling and Completions.* 21 (3): 164-179. SPE-90904-PA. https://doi.org/10.2118/90904-PA.

Klever, F.J. and Stewart, G. 1998. Analytical Burst Strength Prediction of OCTG With and Without Defects. Paper presented at SPE Applied Technology Workshop on Risk Based Design of Well Casing and Tubing, The Woodlands, Texas, USA, 7-8 May. SPE-48329-MS. https://doi.org/10.2118/48329-MS.

Ludwik, P. Elem. Technol. Mech. Springer Verlag, Berlin (1909).

MacDonald, W.D. and Gram, M. 2021. Titanium Casing for High Temperature Wells. Presented at the 2021 Geothermal Rising Conference, Virtual, 3–6 October. In *GRC Transactions*, Vol. 45, 203–221. Mount Laurel, New Jersey, USA: Geothermal Rising.

Maruyama, K., Tsuru, E., Ogasawara, M. et al. 1990. An Experimental Study of Casing Performance Under Thermal Cycling Conditions. SPE Drilling Eng 5 (2): 156-164. SPE-18776-PA. https://doi.org/10.2118/18776-PA.

Nowinka, J., Kaiser, T. and Lepper, B. 2007. Strain-Based Design of Tubulars for Extreme Service Wells. Paper presented at the SPE/IADC Drilling Conference, Amsterdam, The Netherlands, 20-22 February. SPE-105717-MS. https://doi.org/10.2118/105717-MS.

Standards New Zealand. Code of practice for deep geothermal wells. 2015. Wellington (NZ): Standards New Zealand. NZS 2403:2015.

Stewart G, Klever F, Ritchie D. An analytical model to predict the burst capacity of pipelines. Proceedings of Offshore Mechanics and Arctic Engineering (OMAE). Houston (TX): American Society of Mechanical Engineers; 1994. 5:177–88.

Tao, G., Abdulhameed, D., MacDonald, W., Dunlap, D. and Elder, R. 2022. Feasibility study of premium casing connection with titanium alloy for high-temperature geothermal applications. Proceedings of the SPE Thermal Well Integrity and Production Symposium; 2022 Nov 20 - Dec 1; Banff, AB. Richardson (TX): Society of Petroleum Engineers. SPE 212141.

Tao, G. 2023. Effect of stress-strain curve on burst pressure prediction for pipelines with and without corrosion defects. Proceedings of the ASME 2023 Pressure Vessels & Piping

Conference; 2023 July 16-21; Atlanta, GA. New York (NY): American Society of Mechanical Engineers.

Tao, G., Matthews, C., and Adams, A. 2021. Special Considerations for Well Tubular Design at Elevated Temperatures. *SPE Drilling and Completions*. 36 (2): 300–319. SPE 199570-PA. https://doi.org/10.2118/199570-PA.

Zhu, X. and Leis, B.N. 2006. Average shear stress yield criterion and its application to plastic collapse analysis of pipelines. International Journal of Pressure Vessels Piping Vol. 83: pp. 663-71.